Microfluidic Encapsulation of Prickly Zinc-Doped Copper Oxide Nanoparticles with VD1142 Modified Spermine Acetalated Dextran for Efficient Cancer Therapy

Hongbo Zhang, Dongfei Liu, Liang Wang, Zehua Liu, Runrun Wu, Agne Janoniene, Ming Ma, Guoqing Pan, Lina Baranauskiene, Linlin Zhang, Wenguo Cui, Vilma Petrikaite, Daumantas Matulis, Hongxia Zhao, Jianming Pan,* and Hélder A. Santos**

Structural features of nanoparticles have recently been explored for different types of applications. To explore specific particles as nanomedicine and physically destroy cancer is interesting, which might avoid many obstacles in cancer treatment, for example, drug resistance. However, one key element and technical challenge of those systems is to selectively target them to cancer cells. As a proof-of-concept, Prickly zinc-doped copper oxide (Zn–CuO) nanoparticles (Prickly NPs) have been synthesized, and subsequently encapsulated in a pH-responsive polymer; and the surface has been modified with a novel synthesized ligand, 3-(cyclooctylamino)-2,5,6-trifluoro-4-[(2-hydroxyethyl)sulfonyl] benzenesulfonamide (VD1142). The Prickly NPs exhibit very effective cancer cell antiproliferative capability. Moreover, the polymer encapsulation shields the Prickly NPs from unspecific nanopiercing and, most importantly, VD1142 endows the engineered NPs to specifically target to the carbonic anhydrase IX, a transmembrane protein overexpressed in a wide variety of cancer tumors. Intracellularly, the Prickly NPs disintegrate into small pieces that upon endosomal escape cause severe damage to the endoplasmic reticulum and mitochondria of the cells. The engineered Prickly NP is promising in efficient and targeted cancer treatment and it opens new avenue in nanomedication.

1. Introduction

Cancer is a very complex and serious disease that greatly threatens human health and challenges the current medication.[1–6] The severe side effects of anticancer drugs and multiple biological barriers tremendously hindered the therapeutically efficiency of cancer.[1] Owning to the intratumoral heterogeneity of cancers[2] and individual differences in patients,[3] it is very difficult to unravel the mysteries of cancers and make intuitive drug design.[4] It is almost impossible to find an omnipotence drug for versatile types of cancers and for all patients.[5] Moreover, the continuous dosing of drugs will lead to multiple drug resistance (MDR), which is one of the major clinical problems for successful

Prof. H. Zhang,[+] Dr. D. Liu, Z. Liu, Prof. H. A. Santos
Division of Pharmaceutical Chemistry and Technology
Faculty of Pharmacy
University of Helsinki
FI-00014 Helsinki, Finland
E-mail: hongbo.zhang@abo.fi; helder.santos@helsinki.fi

Prof. H. Zhang
Harvard John A. Paulson School of Applied Science and Engineering
Harvard University
Cambridge, MA 02138, USA

L. Wang, Dr. H. Zhao
Institute of Biotechnology
University of Helsinki
FI-00014 Helsinki, Finland

R. Wu. Prof. J. Pan
School of Chemistry and Chemical Engineering
Jiangsu University
Zhenjiang 212013, China
E-mail: jsdxpjm@126.com

A. Janoniene, Dr. L. Baranauskiene, Dr. V. Petrikaite, Prof. D. Matulis
Department of Biothermodynamics and Drug Design
Institute of Biotechnology
Vilnius University
LT-10257 Vilnius, Lithuania

Dr. M. Ma, Dr. L. Zhang
Shanghai Institute of Ceramics
Chinese Academy of Sciences
Shanghai 200050, China

Dr. G. Pan, Prof. W. Cui
Department of Orthopaedics
The First Affiliated Hospital of Soochow University
Orthopaedic Institute
Soochow University
Suzhou 215006, China

V. Petrikaite
Department of Drug chemistry
Faculty of Pharmacy
Lithuanian University of Health Sciences
LT-44307 Kaunas, Lithuania

Prof. J. Pan
Department of Chemistry
Stanford University
Stanford, CA 94305, USA

[+]Present address: Department of Pharmaceutical Sciences Laboratory, Åbo Akademi University, FI-20520, Turku, Finland

DOI: 10.1002/adhm.201601406

cancer treatment.[7,8] Nanotechnology has shown advantages in cancer treatment.[9] Different types of nanoparticles have been developed to enhance the targeting selectivity of drugs and to assist the drugs to cross biological barriers and specific barriers in tumors.[10] These nanoparticles play the role as vectors to deliver the drugs.[9] However, the active pharmaceutical ingredients are drugs and many obstacles in drug based cancer treatment still exist, for example, the development of drug resistance in cancer. The exploring of nanoparticles as nanomedicine to combat cancer is attractive and may open new avenue for effective cancer treatment.[1] Recently, several studies have shown that certain nanoparticles lead to cancer cells death in the absence of drug.[11,12] For instance, plasmonic nanobubbles can kill cancer cells through laser induced photothermal therapy.[12] However, the treatment relies on laser, which is technically difficult to be applied to patients, especially for treating tumors from different organs that are very deep in human body. Zinc–copper oxide nanoparticles lead to cancer cell death, but have no targeting effect.[13] Moreover, the therapeutic efficiency of these treatments is often not strong enough, and thus, drugs are added as a combination therapy.

The inspiration of using nanoparticles with special nanostructures for cancer treatment comes from their recent applications in combating bacterial. Graphene oxides nanosheets induced membrane stress by the sharp edges and led to the loss of bacterial membrane integrity, thus killed the bacteria.[14] The silica nanopollens can enhance bacterial adhesion and inhibit bacterial proliferation for long term.[15] The killing mechanism of those platforms is primarily through physical disruption instead of chemical induction, thus can eliminate the obstacles of MDR in bacteria killing.[14,15] However, these platforms cannot be directly translated to cancer treatment since they are dangerous for human body, which basically destroy all cells when in contact.

Microfluidic technology is very promising for both nano- and microfabrication and encapsulation, owning to its advanced properties, including high encapsulation efficiency, monodispersed size of fabricated particles, batch-to-batch reproducibility, and industrial scale production.[16–18] Microfluidic nanoprecipitation device can encapsulate the NPs with full protection.[19,20] The acid-degradable acetylated dextran (AcDX)[21,22] dissolves in mild acidic conditions, such as lysosome in the cells.[20–22] Spermine-modified acetalated dextran (SpAcDX) inherits the pH responsiveness of AcDX and the termini NH_2 groups are more reactive and ready for further chemical conjugation. SpAcDX NP is very promising for intracellular delivery of payloads, which has been applied to deliver siRNA to cancer cells with low cytotoxicity.[23]

Carbonic anhydrase IX (CA IX) is considered to be a very good cancer tumor marker since it is highly expressed in tumor tissues and very limited expressed in normal tissues.[24,25] CA IX catalyses the conversion between carbon dioxide and bicarbonate, and it is critical for cancer cell survival, especially under hypoxia conditions.[24] CA IX also plays a vital role in cancer cell migration, invasion, and in the increased tumor resistance to chemo- and radiotherapy.[26,27] 3-(Cyclooctylamino)-2,5,6-trifluoro-4-[(2-hydroxyethyl)sulfonyl] benzenesulfonamide (VD1142) is a CA IX inhibitor with high selectivity and the mechanism of recognition relies on the high binding affinity.[28,29] Thus, it might also act as a potential CA IX targeting ligand when conjugating to nanoparticles. Due to the specific expression of CA IX in tumor, the evaluation of VD1142 as a ligand for cancer targeting is scientifically important. Polyethylene glycol (PEG) has been widely used as a linker for ligand conjugation and the PEG coating can significantly decrease the unspecific intracellular uptake.[30]

Herein, for the first time, we encapsulated the Prickly Zn–CuO NPs (Prickly NP) in SpAcDX and further modified the surface with VD1142 through a PEG linker. The developed nanocomposite, named as Prickly@SpAcDX–PEG–VD1142, is throughout evaluated for its cancer cell antiproliferative capability, CA IX targeting selectivity, intracellular distribution, and mechanism of inducing MCF-7 breast cancer cells death (**Scheme 1**).

2. Results and Discussion

2.1. Fabrication and Characterization of Prickly Zn–CuO NPs

A green sonochemical method was applied to synthesis the Prickly Zn–CuO NPs in water/alcohol mixture solution (1:9).[31] The high resolution transmission electron microscopy (HR-TEM) images indicated that the obtained Prickly Zn–CuO NPs had narrow size distribution and possessed multiple exterior pricks (**Figure 1**A and Figure S1A, Supporting Information). Under reverted water/alcohol solution (9:1), we also successfully synthesized needle Zn–CuO with only two sharp tips (Figure S1B, Supporting Information),[31] which was attributed to the solvent polarity-induced nanoparticle deposition and growth.[32] As measured from dynamic light scattering (DLS), the Prickly NP was 144 ± 1 nm with a polydispersity index (PDI) of 0.1, and had a zeta (ζ)-potential of 5.9 ± 1.8 mV (Table S1, Supporting Information).

The Prickly NP was formed at 0.015 M of total ion concentration under 750 W sonochemical irradiation intensity for 1 h.[31] The formation followed time-dependent nanocrystal growth and nanocrystal deposition growth of nanopricks, from nanoclusters (Figure S1A,B, Supporting Information) to robust Prickly NP (Figure 1A). Additionally, high ion concentration of 0.015 M (Figure S1C,D, Supporting Information and Figure 1A) and high enough sonochemical irradiation intensity (750 W) were needed for the formation of Prickly NP (Figure S2E,F, Supporting Information and Figure 1A).

The Prickly NP was characterized by X-ray photoelectron spectroscopy (XPS) and X-ray diffraction (XRD). The binding energy at 933–934 eV for Cu $2p_{3/2}$, the vibration peak at 940–944 eV, and the binding energy at 951–955 eV for Cu $2p_{1/2}$ were corresponding to the three major XPS characteristics of Cu element,[33] and the peaks of Zn $2p_{3/2}$, Zn $2p_{1/2}$, were obtained at 1021–1022 and 1043–1044 eV, respectively in XPS (Figure S2C, Supporting Information).[34] In XRD, characteristic peaks at 2θ = 32.47°, 35.49°, 38.68°, 48.65°, 58.25°, 61.45°, 66.51°, 67.85°, and 75.10° (Figure S2E, Supporting Information), which represented typical monoclinic CuO, were observed (standard Joint Committee Powder Diffraction Standards No. 80-1916).[35] Additionally, in the HR-TEM images of Prickly

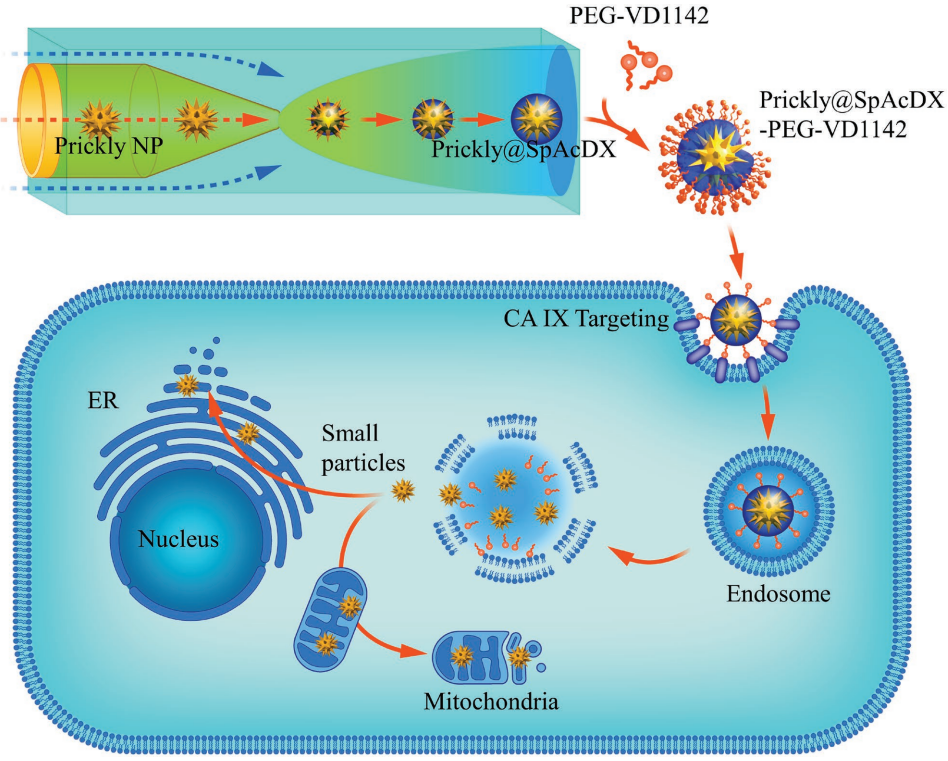

Scheme 1. Schematic illustration of the efficient targeting of cancer cells and the antiproliferative effect by the engineered Prickly@SpAcDX–PEG–VD1142 particles fabricated by microfluidic encapsulation of Prickly NPs in SpAcDX nanomatrix, and subsequently surface conjugated with PEG-VD1142. The intracellular distribution and structural regulated nanopiercing of ER and mitochondria in cancer cells are also highlighted.

NP (Figure 1A), ultrasmall nanoclusters other than traditional single crystals were shown and the bending/wrinkling/crossing of the lattice fringes caused by the stacking faults in the atomic rows were found in many lattice areas with obvious distortions, indicating their intrinsic dopant state (Figure 1A, white circles). The energy-dispersive X-ray spectroscopy elemental mapping in **Figure 2**A demonstrated that Zn atoms were doped and located within the bulk of the CuO crystals. A composition of 86% of Cu and 11% of Zn was found in Prickly NP as quantified via inductively coupled plasma mass spectrometry (ICP-MS) (Table S2, Supporting Information). The characterization results are in good agreement with our previous study,[31] which revealed the successful synthesis of Prickly Zn doped CuO nanoparticles in this work.

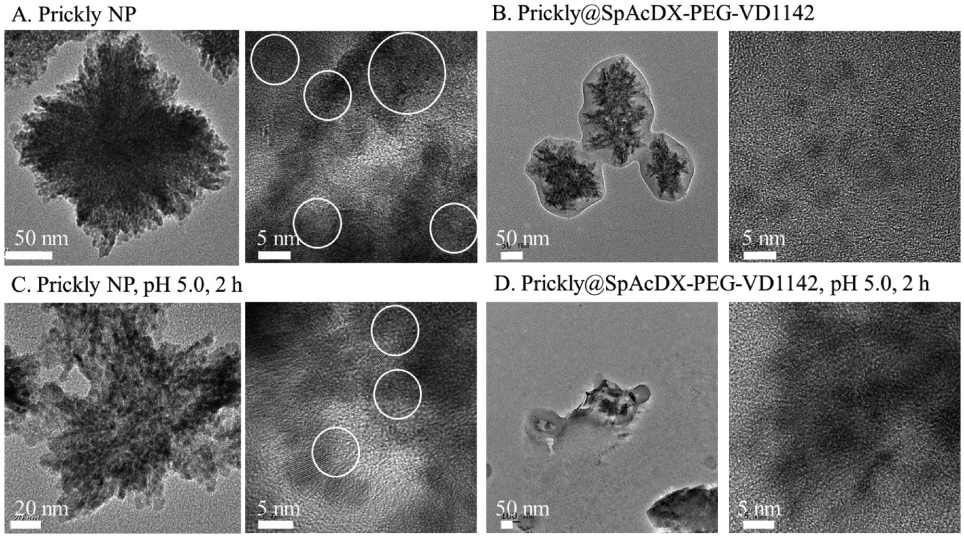

Figure 1. HR-TEM images and the high magnification lattice structure of A) Prickly NP, B) Prickly@SpAcDX–PEG–VD1142, C) Prickly NP at pH 5.0 for 2 h, and D) Prickly@SpAcDX–PEG–VD1142 at pH 5.0 for 2 h. White circles in (A) indicate the bending/wrinkling/crossing of the lattice fringes.

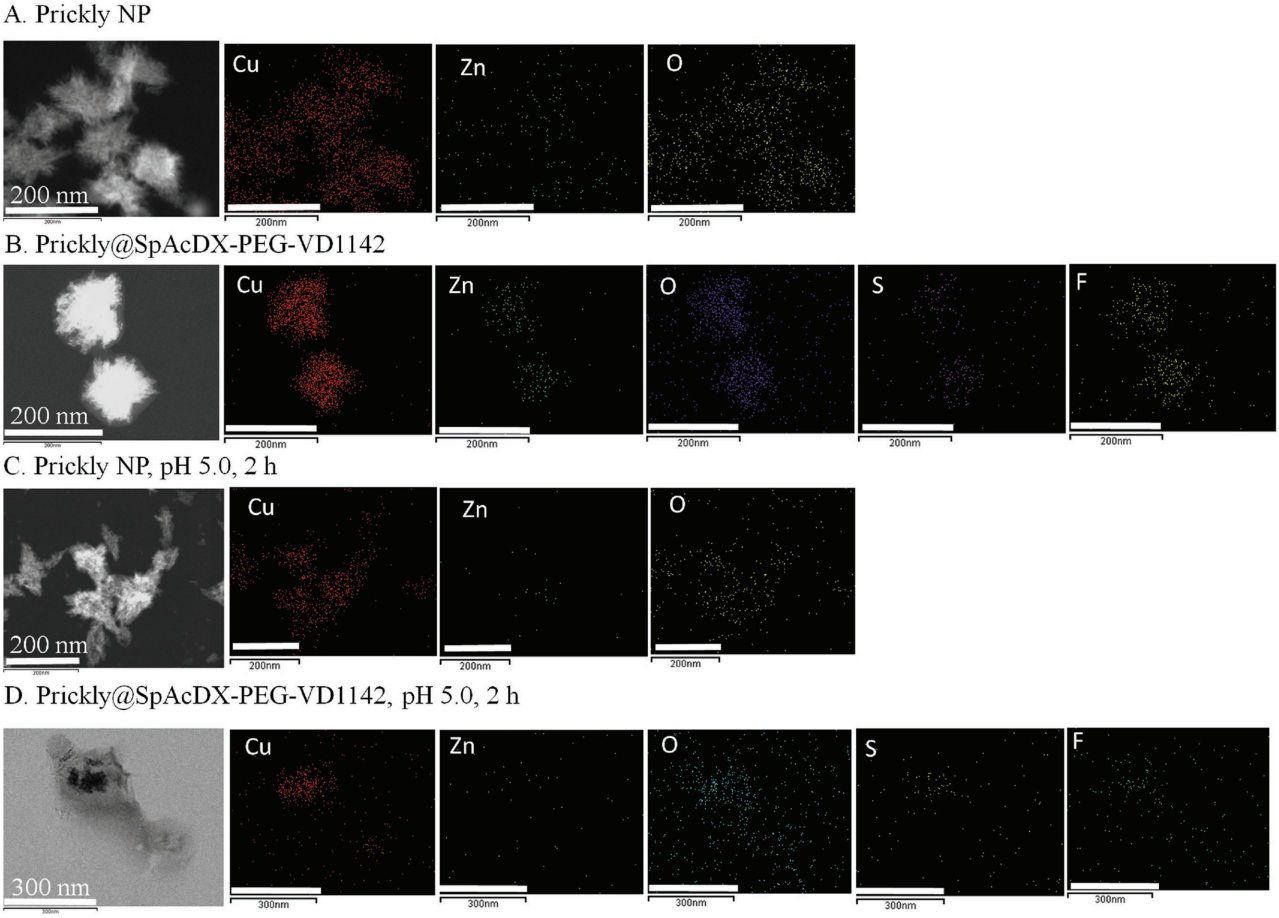

Figure 2. HR-TEM EDX mapping of A) Prickly NP, B) Prickly@SpAcDX–PEG–VD1142, C) Prickly NP at pH 5.0 for 2 h, and D) Prickly@SpAcDX–PEG–VD1142 at pH 5.0 for 2 h. For Prickly NPs, the Cu, Zn, and O elements are mapped; for Prickly@SpAcDX–PEG–VD1142, the Cu, Zn, O, S, and F elements are mapped.

2.2. Encapsulation of Prickly NPs with SpAcDX and Conjugation of VD1142

The Prickly NPs were encapsulated with SpAcDX using microfluidic nanoprecipitation in order to shield the NPs from unspecific attacking to the CA IX negative cells. The Prickly NPs and SpAcDX (1:5) were mixed by sonication in ethanol and pumped through the microfluidics inner capillary. As outer flow, 1% of poly(vinyl alcohol) (PVA) was dissolved in MilliQ-water and the pH was adjusted to 8, because both Prickly and SpAcDX NPs are sensitive to acidic conditions. At the site of the orifice, the inner flow was rapidly diffused to the miscible outer flow and the precipitation process initiates with supersaturation, and thus, lead to nucleation and NPs' formation (Scheme 1). In the presence of Prickly NPs, the nucleation happened at the surface of these particles and led to the polymeric encapsulation. As described in our previous study, the layer thickness and encapsulation efficiency are adjustable by changing the concentration of the NP and polymer, and the flow ratio and flow rates of the two flows, etc.[20] In this work, we found that the Prickly NP to SpAcDX ratio of 1:5 and the flow rates of 2:40 mL h^{-1} were the optimal conditions for efficient encapsulation (data not shown). The Prickly@SpAcDX was 226 nm (PDI = 0.17) with ζ-potential of +41 mV.

To conjugate the ligand VD1142 (Figure S3A, Supporting Information), NH_2–PEG–COOH (molecular weight, MW 5000) was selected as a linker. The –OH group of VD1142 was first reacted with the $-NH_2$ group of PEG through the carbonyldiimidazole (CDI) mediated amide coupling reaction in toluene, which blocked the $-NH_2$ groups in PEG and prevented unspecific self-conjugation between the −COOH and $-NH_2$ groups within the PEG molecule in the following step. After removal of toluene, the HOOC−PEG−VD1142 was resuspended in 2-[4-(2-hydroxyethyl)piperazin-1-yl]ethanesulfonic acid (HEPES) buffer and conjugated with the $-NH_2$ group on Prickly@SpAcDX through 1-ethyl-3-(3-dimethylaminopropyl) carbodiimide/*N*-hydroxysuccinimide (EDC/NHS) coupling reaction. Interestingly, the polymer layer became thicker after conjugation of PEG–VD1142 (Figure 1B), with particle size increased to 274 nm and ζ-potential decreased to +7 mV (Table S1, Supporting Information). Moreover, as indicated in Figure S4 and Table S1 in the Supporting Information, the Prickly@SpAcDX–PEG–VD1142 particles had good monodispersity and no free Prickly NPs were observed

in the sample (Figure S4A–C, Supporting Information). In addition, the prickly structure was fully encapsulated inside the SpAcDX polymeric matrix (Figure S4D, Supporting Information). Notably, we are the first to discover the fluorescent property of VD1142 (Figure S3B, Supporting Information). The successful conjugation of VD1142 on Prickly@SpAcDX was evaluated and quantified by fluorescent at Ex/Em of 360/490 nm as indicated in the VD1142 fluorescence spectrum (Figure S3B, Supporting Information). The results showed that Prickly@SpAcDX–PEG–VD1142 contained 1.2% (weight ratio) of VD1142. And by calculating the weight change, PEG accounted for 22% of the total particle weight. The presence of VD1142 on the surface of Prickly@SpAcDX–PEG–VD1142 particles was also confirmed with Fourier transform infrared spectroscopy (FTIR), for which many of the VD1142 peaks were observed in the Prickly@SpAcDX–PEG–VD1142 (Figure S5, Supporting Information). In addition, from energy-dispersive X-ray (EDX) spectroscopy mapping (Figure 2B), fluoride (F), and sulfur (S) elements (specific elements only exist on VD1142) were detected and had uniform distribution on the particles, which demonstrated the successful and well dispersible conjugation of VD1142 on the surface of Prickly@SpAcDX particles (Figure 2B).

2.3. Dissolution of the Prickly NP in Lysosomal pH

Copper based NPs are unstable in acidic conditions.[36] Here, we monitored the dissolution behavior by incubating the Prickly NPs at pH 5 for 2 h, mimicking the intracellular pH inside the lysosomes. Interestingly, the Prickly NPs disintegrated to small pieces and the rough structure still remained at some extend (Figure 1C). No significant lattice fringe changes were observed after dissolving the NPs (Figure 1A,C). However, the EDX mapping indicated the obvious decrease of Zn content after acid incubation (Figure 2A,C). The special dissolution behavior of the Prickly NP was due to the unique formation mechanism, as described above (Figure S1, Supporting Information and Figure 1A). In addition, due to the vulnerable nature of Zn^{2+}, its existence facilitated the abrupt disintegration of Prickly NPs to ultrasmall particles.[37] In the case of Prickly@SpAcDX–PEG–VD1142, both polymer layer and the encapsulated Prickly NP dissolve in acidic pH (Figure 1D). The F and S elements were found at the site of the dissolved polymers, which indicated the presence of VD1142 on the dissolved polymers (Figure 2D). Further incubation of the Prickly NP at pH 5 resulted in fully dissolving of those particles (Figure S6, Supporting Information).

2.4. Targeting Capability of Prickly@SpAcDX–PEG–VD1142 to CA IX Expressed Cancer Cells

To explore the targeting capability of Prickly@SpAcDX–PEG–VD1142 to cancer cells, we carried out a fluorescent thermal shift assay (FTSA, also called ThermoFluor and Differential Scanning Fluorimetry).[38–40] The Prickly@SpAcDX was conjugated with HOOC–PEG–methoxyl (MW 5000), named as Prickly@SpAcDX–PEG, to act as control for evaluating the effect of the conjugated ligand, VD1142. The binding of Prickly NPs, Prickly@SpAcDX–PEG, Prickly@SpAcDX–PEG–VD1142, and free VD1142 to CA IX protein were compared. In the presence of increasing concentrations of VD1142, the T_m value (protein melting temperature)[38–40] had an increase of up to ≈15 °C, indicating a very strong protein binding (**Figure 3**A). Interestingly, Prickly@SpAcDX–PEG–VD1142 behaved almost the same as free VD1142 (Figure 3A), whereas in the case of Prickly NPs and Prickly@SpAcDX–PEG, almost no T_m shift (up to only 1 °C using the same concentrations) was observed (Figure 3A). Therefore, the unspecific binding of Prickly NPs is eliminated, proving that the conjugation of VD1142 endowed the Prickly@SpAcDX–PEG–VD1142 with CA IX targeting capacity.

In addition to the binding assay, the CA IX protein inhibition was studied by the stopped-flow CO_2 hydration method.[41] The CA IX protein activity was plotted in the presence of different inhibitors (Prickly@SpAcDX–PEG, Prickly@SpAcDX–PEG–VD1142, and free VD1142) at different concentrations in log scale. As a result, the Prickly@SpAcDX–PEG–VD1142 inhibited CA IX activity similarly to free VD1142, whereas Prickly@SpAcDX–PEG had no inhibition effect (Figure 3B). These results further confirmed that the VD1142 conjugation led to CA IX protein targeting.

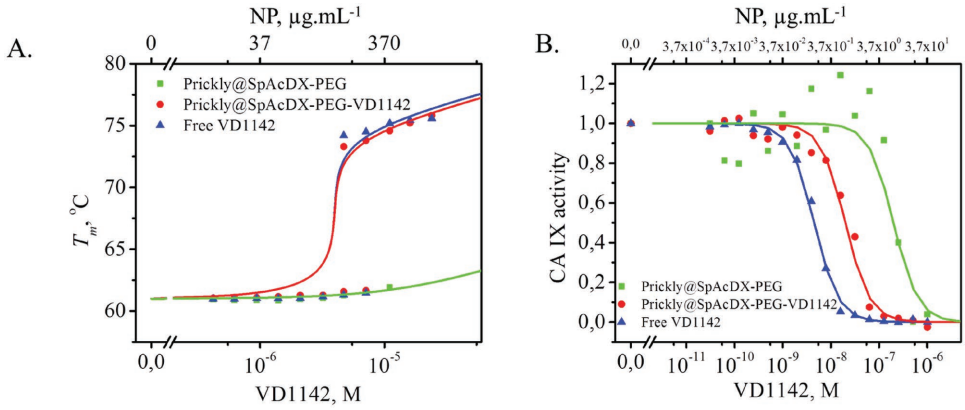

Figure 3. The CA IX binding and inhibition of the Prickly NPs and Prickly@SpAcDX–PEG–VD1142. A) Protein binding assay toward CA IX. B) Protein inhibition assay toward CA IX. The particle concentration is calculated based on VD1142 conjugation degree of 1.2%.

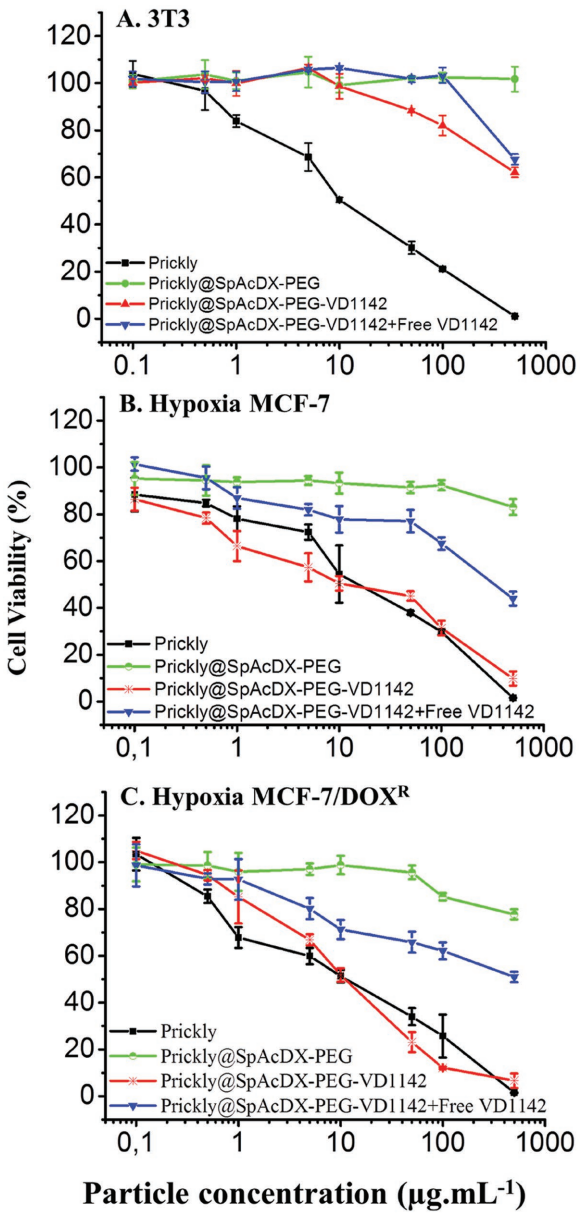

Figure 4. Cell viability assays toward A) 3T3, B) MCF-7 under hypoxia condition, C) MCF-7/DOX^R under hypoxia condition. The cells were incubated with prickly, Prickly@SpAcDX–PEG, Prickly@SpAcDX–PEG–VD1142. In Prickly@SpAcDX–PEG–VD1142 + Free VD1142 group, the cells were incubated with 10 μg mL^{-1} free VD1142 and the particles.

2.5. Antiproliferative Cancer Cell Studies

The in vitro antiproliferative capability and selectivity of the Prickly@SpAcDX–PEG–VD1142 on CA IX overexpressed cells were evaluated with a cell viability assay (**Figure 4**). The 3T3 fibroblast cells[42] and hypoxia MCF-7 cells[43] (chemically induced by $CoCl_2$ for 48 h)[44] (Figure S7, Supporting Information) were selected to represent CA IX negative and CA IX positive cells.[42,43] As observed in Figure 4A,B, the Prickly NPs were very effective on inhibiting the cell proliferation regardless of cell type tested. Notably, the encapsulation with SpAcDX and the subsequent PEG conjugation (Prickly@SpAcDX–PEG) was able to shield the Prickly NPs and significantly reduced the cell killing in all cell types (Figure 4B). Most importantly, the selective antiproliferative effect was found with Prickly@SpAcDX–PEG–VD1142, which exhibited much stronger antiproliferative activity toward hypoxia MCF-7 over 3T3 cells. In the presence of free VD1142, VD1142 acted as competitor that inhibited CA IX, and the antiproliferative activity of Prickly@SpAcDX–PEG-VD11 was inhibited, which demonstrated that the CA IX positive cells recognition was through VD1142 mediated CA IX protein targeting. Prickly NPs and Prickly@SpAcDX–PEG–VD1142 showed similar efficacy on inhibiting the hypoxia doxorubicin (DOX) resistant MCF-7 cells (MCF-7/DOX^R) proliferation (Figure 4C), indicating that the Prickly NPs could reduce the MDR. In comparison to the prickly nanodiamonds,[45] the Prickly NPs in this study are more effective in inducing cancer cell death, which might owe to the special elemental composition and other properties of those particles.

2.6. Intracellular Uptake and Distribution

The intracellular distribution of the Prickly@SpAcDX–PEG–VD1142 in hypoxia MCF-7 breast cancer cells[43] (chemically induced by cobalt(II) chloride, $CoCl_2$) (Figure S7, Supporting Information) was investigated by confocal fluorescence microscopy. To avoid massive cell death at 24 h, the Prickly NPs and Prickly@SpAcDX–PEG–VD1142 were incubated with MCF-7 cells for 3 h and then replaced with cell medium for another 21 h. VD1142 has blue fluorescence by itself (Figure S3B, Supporting Information). The Prickly NPs were surface modified with (3-aminopropyl)triethoxysilane and then conjugated with NHS-fluorescein to obtain green fluorescence, and the MCF-7 cells were stained with lysotracker red. At 2 h of incubation, the Prickly@SpAcDX–PEG–VD1142 accumulated on the cell membrane: an overlap of green and blue fluorescence revealed the colocalization of Prickly NPs with SpAcDX–PEG–VD1142 layer (Video S1, Supporting Information). After 12 h, some of the Prickly@SpAcDX–PEG–VD1142 NPs were internalized and the separation of green and blue fluorescence indicated the dissolution of SpAcDX–PEG–VD1142 layer (Video S2, Supporting Information). After 24 h, many Prickly@SpAcDX–PEG–VD1142 were taken-up by the cell and the free Prickly NPs were found inside the cells as free green particles (Video S3, Supporting Information and **Figure 5**). The Prickly NP and Prickly@SpAcDX–PEG–VD1142 behaved similarly in intracellular uptake and endosomal escape (Figure 5). The Prickly NP (green) and lysosome (red) colocalization was analyzed by Imaris software and the calculated Pearson's correlation coefficient was 0.56 ± 0.06 (n > 10) for Prickly NP and 0.35 ± 0.06 (n > 10) for Prickly@SpAcDX–PEG–VD1142.

Next, flow cytometry was used to quantitatively evaluate and compare the interaction of Prickly NPs, Prickly@SpAcDX–PEG and Prickly@SpAcDX–PEG–VD1142 particles with hypoxia MCF-7 cells. The signals of all samples were acquired based on the green fluorescein conjugated to Prickly NPs. The obtained histograms and calculated fluorescent intensity (Figure S8,

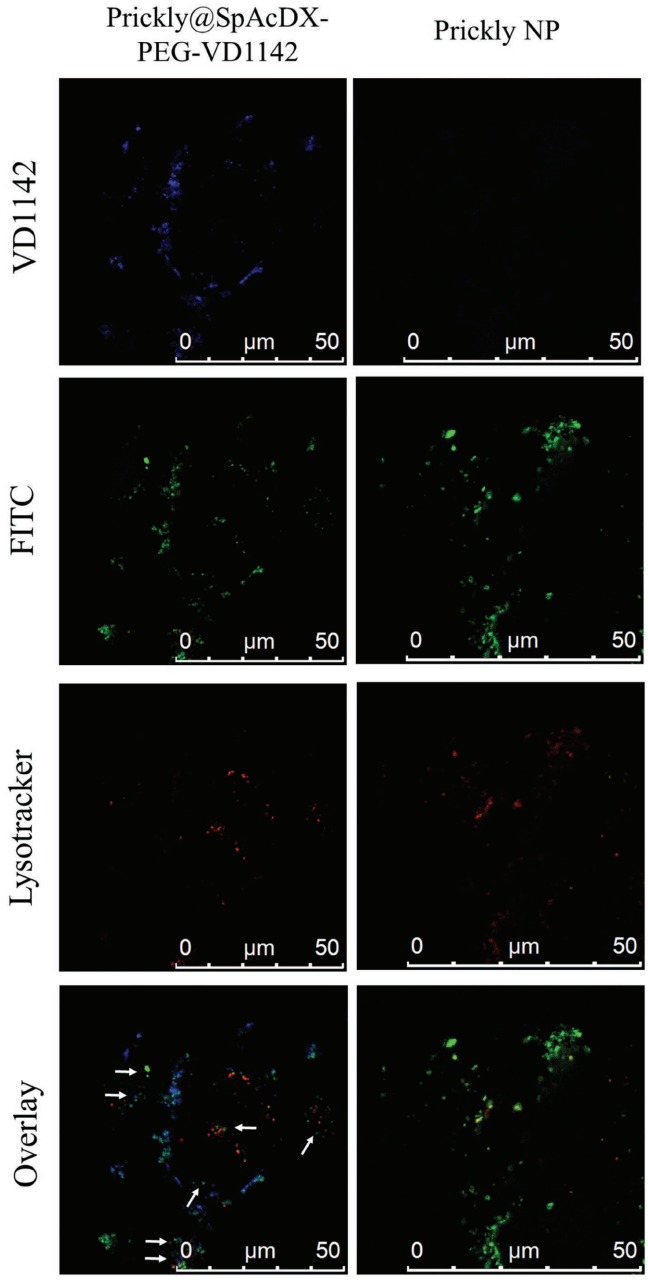

Figure 5. Confocal microscopy analysis of the intracellular uptake and endosomal escape of Prickly NPs and Prickly@SpAcDX–PEG–VD1142 in MCF-7 breast cancer cells under hypoxia conditions. VD1142 had blue fluorescence, Prickly NPs were labeled in green and lysosomes were labeled in red fluorescence. White arrows indicate the green particles that did not overlay with blue and red. The particles (10 μg mL^{-1}) were incubated with MCF-7 cells under hypoxia condition for 3 h and then the cells were incubated with medium for another 21 h.

Supporting Information) indicated that the Prickly NPs and Prickly@SpAcDX–PEG–VD1142 had strong interaction with the MCF-7 cells, while Prickly@SpAcDX–PEG did not. This is because that PEG coating can significantly reduce unspecific cellular uptake.[46] However, the mechanism of cellular interaction between the Prickly NPs and Prickly@SpAcDX–PEG–VD1142 were different. As indicated by the protein binding assay, the Prickly NPs had no binding affinity to CA IX (Figure 3) and the cellular interaction was most probably through direct punching the cell with the prickly structure, whereas after SpAcDX and PEG encapsulation, the unspecific cellular interaction was inhibited and Prickly@SpAcDX–PEG showed limited cellular interaction (Figure S8, Supporting Information). Interestingly, after conjugating VD1142, the Prickly@SpAcDX–PEG–VD1142 showed high CA IX binding and also good interaction with hypoxia MCF-7 cells that express CA IX (Figures S7 and S8, Supporting Information). Therefore, Prickly@SpAcDX–PEG–VD1142 had much better selectivity and targeting ability than Prickly NPs to cells expressing CA IX.

The Prickly@SpAcDX–PEG–VD1142 distribution in hypoxia MCF-7 breast cancer cells[43] was further confirmed by TEM (same conditions as for confocal and flow cytometry). Notably, the Prickly@SpAcDX–PEG–VD1142 were extensively taken-up by the endosomes/lysosomes of the cells and the SpAcDX–PEG-VD1142 layer was dissolved inside those cellular compartments (**Figure 6**B).[23,45] Subsequently, we noticed that most of the Prickly NPs escaped from endosome disintegrated into small pieces. Under the conditions of the dissolution experiments (Figure 1C,D) and what we observed inside the cells (Figure 6), we believe that the Prickly NPs in fact underwent disintegration upon endocytosis and endosomal escape process, and the ultrasmall particles induced extra deleterious effects toward subsequent destruction of the cellular organelles. As shown in Figure 6C,D, many of the ultrasmall particles were observed in mitochondria, which resulted in mitochondrial membrane disruption and fragmentation. It has been previous reported that prickly nanodiamonds could escape from endosome,[45] however those particles was not found to accumulate in mitochondria. Thus, the specific intracellular distribution of Prickly particles used in this study is probably benefited from the unique material composition, surface roughness and size transformation to ultrasmall particles.[47] Similar intracellular distribution was found for Prickly NPs without encapsulation (Figure S9, Supporting Information).

2.7. Mechanism of Antiproliferative Effect

In order to uncover the mechanism of MCF-7 cells death after incubating with Prickly@SpAcDX–PEG-VD1142, the morphology changes of the mitochondria and endoplasmic reticulum (ER) were assessed by immunofluorescence microscopy. The MCF-7 cells were stained with antibody against Tom20,[48] a mitochondrial outer membrane protein, and calreticulin, which is a calcium-binding protein mainly localized in the ER lumen.[49] As shown in **Figure 7**A, Prickly NPs and Prickly@SpAcDX–PEG–VD1142 led to obvious morphology change of the mitochondria from regular tubular structure to swollen and fragmented structure (Figure 7A), which clearly indicates the mitochondrial damage.[50] In addition, they also caused fragmentation of the ER network (Figure 7B).[51] Apoptotic relative proteins, 19 and 17 kDa fragments of cleaved caspase-3 (active form of caspase-3) are key executioners of apoptosis responsible for the proteolytic cleavage of many key proteins, such as the nuclear enzyme poly (adenosine diphosphate-ribose) polymerase (PARP).[52] We have analyzed

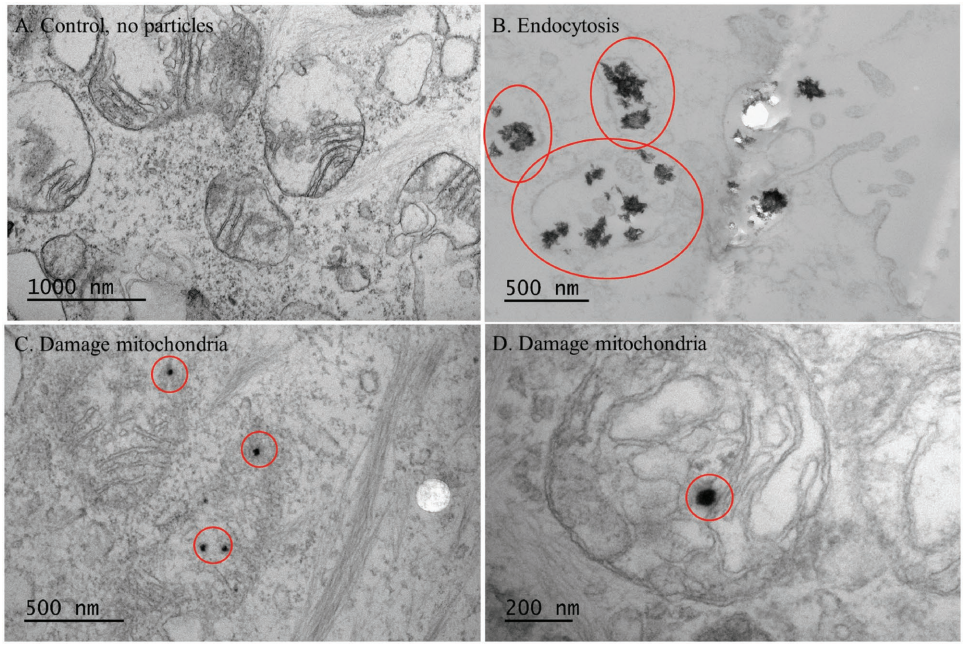

Figure 6. TEM tracking of the Prickly@SpAcDX–PEG–VD1142 inside the MCF-7 cells under hypoxia condition. The Prickly NPs and broken small crystals were highlighted with red circles. The particles (10 μg mL^{-1}) were incubated with MCF-7 cells under hypoxia condition for 3 h and then the cells were incubated with medium for another 21 h.

whether Prickly NPs activated this pathway by western blotting.[52] Interestingly, the results showed that in contrast to valinomycin[53] (positive control) and fully dissolved Prickly@SpAcDX–PEG–VD1142 solution, Prickly NPs and Prickly@SpAcDX–PEG–VD1142 did not lead to the expression of 19- and 17-kDa fragments of cleaved caspase-3 (active form of caspase-3) (**Figure 8**), and the nuclear enzyme PARP did not decrease.[54,55] Conversely, in the valinomycin and dissolved particle groups, the expression level of PARP was much lower and cleaved caspase-3 was much higher than in Prickly NPs and Prickly@SpAcDX–PEG–VD1142 treated groups (Figure 8). Therefore, the Prickly NPs and Prickly@SpAcDX–PEG–VD1142 merely did not induce caspase mediated apoptotic cell death. Caspase-dependent cell-death played important

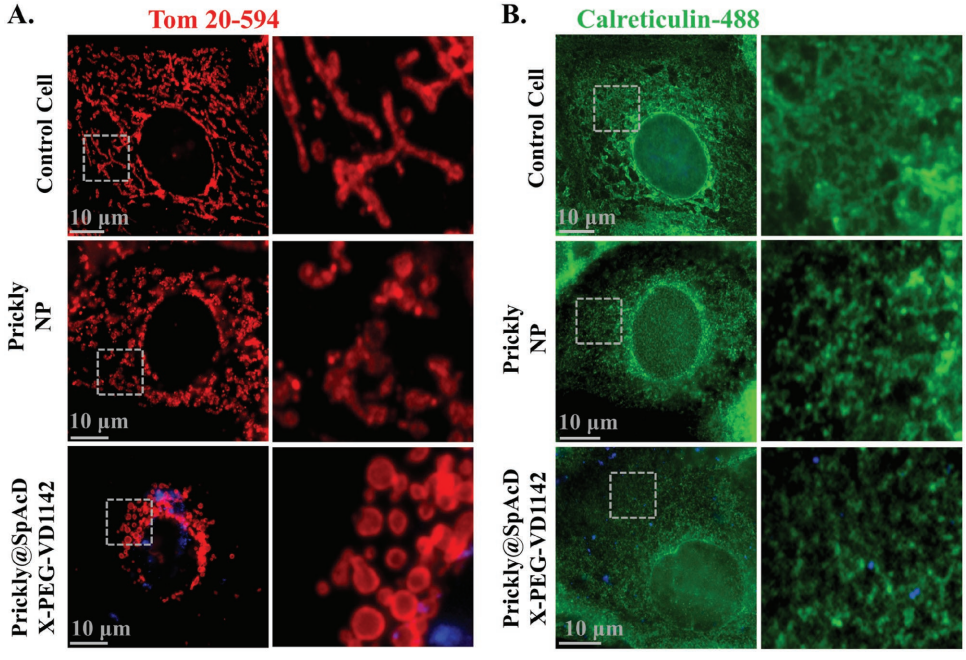

Figure 7. Damage of intracellular organelles. A) Mitochondrial morphology change; Tom20 was labeled with antibody. B) ER morphology change; the calreticulin was labeled with antibody.

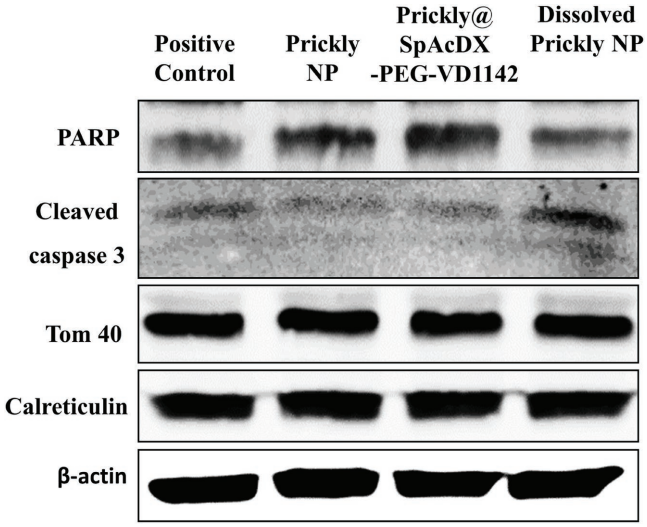

Figure 8. Western blotting of PARP and cleaved caspase 3 expression in response to particle incubation. Tom40 and calreticulin were used as mitochondrial marker and ER marker, respectively. All signals were normalized to β-actin expression level.

role in cancer treatment, however it was also one of the reasons for drug resistance and individual differences in drug response.[56] It has been reported that caspase-independent cell-death processes also exist.[56] In this study, physical nanopiercing induced intracellular damage and directly destroyed the cells in caspase-independent manner, which has great potential in conquering the drug resistance and individual differences and achieving more efficient cancer treatment. In parallel to the western blotting study, release rates of Cu^{2+} inside the cells treated with Prickly NPs and Prickly@SpAcDX–PEG–VD1142 were also determined at 3, 6, and 24 h (Figure S10, Supporting Information). The Cu^{2+} release was less than 5% of the total Cu component for Prickly NPs after 24 h incubation with cells. After encapsulation, the SpAcDX–PEG–VD1142 layer further delayed the Cu^{2+} release, for which only 1.6% of Cu^{2+} was detected at 3 h (Figure S10, Supporting Information).

Finally, it is worth mentioning that we also evaluated the structural relevant antiproliferative effect of the Prickly NPs, needle NPs, and dissolved Prickly NPs toward MCF-7 cells (Figure S11, Supporting Information). Under the same concentration, the Prickly NPs with multidimensional prickly architecture was more effective in inducing cell death than the needle NPs with only two-sharp tips, and much more effective than the dissolved Cu^{2+} with no particle structure (Figure S11, Supporting Information). And in comparison with a recent study using Zn–CuO with no sharp structure, the Prickly NPs were more efficient on inducing cancer cell death.[13] Consequently, we can conclude that the mechanism of antiproliferation in cancer cells is mainly due to structural related physical damage by the Prickly NPs than by the Cu^{2+} ions released induced apoptosis during the NPs' dissolution.

2.8. Human Plasma Stability Analysis

Aggregation is often a big problem for nanoparticles and hinders their application in vivo. In vitro plasma stability analysis is an important and easy method to evaluate the nanoparticles' stability and reflect the situation in vivo. In this study, we incubated the Prickly and Prickly@SpAcDX–PEG–VD1142 particles with human plasma at 37 °C and we measured the size and ζ-potential change over time. As a result, the size of the Prickly particles increased from 144 to 210 nm in 5 min and the ζ-potential immediately decreased from +6 to −17 mV in 1 min, and then these values stabilized. This phenomenal indicated that Prickly particles were not very stable and aggregated in human plasma. After SpAcDX–PEG–VD1142 coating, the Prickly@SpAcDX–PEG–VD1142 became more stable and almost did not aggregate in the studied conditions, for which the size slowly increased from 274 to 318 nm in 120 min. The ζ-potential of Prickly@SpAcDX–PEG–VD1142 slowly decreased from +7 to −17 mV in 20 min. These results confirmed that the SpAcDX–PEG–VD1142 coating improved the plasma stability of Prickly particles and the SpAcDX–PEG–VD1142 shell was stable and did not degrade in human plasma. Thus, Prickly@SpAcDX–PEG–VD1142 has a very good potential to be utilized for further in vivo applications (Figure S12, Supporting Information).

3. Conclusion

In summary, we synthesized Prickly Zn–CuO NPs via a facile and environment-friendly fabrication protocol. The Prickly NPs exhibited very efficient anticancer effect, even against DOX resistance breast cancer cells. The microfluidic nanoprecipitation enabled the successful encapsulation of the Prickly NPs and shielded them from unspecific damaging of the receptor negative cells. Moreover, we explored the cancer targeting capability of a novel ligand VD1142 and we successfully witnessed the targeting selectivity of Prickly@SpAcDX–PEG–VD1142 toward CA IX overexpressed hypoxia MCF-7 breast cancer cells. Specifically, the intracellular distribution of the NPs indicated that the Prickly@SpAcDX–PEG–VD1142 induced endosomal escape and, more importantly, they disintegrated into small pieces with extra deleterious effect toward disruption of ER and mitochondrial structures in cells through nanopiercing. By evaluating the protein markers for cell apoptosis and comparing the structurally related cell death, we further confirmed that the anticancer mechanism was mainly due to physical damage of the cells instead of Cu^{2+} induced toxicity. Overall, we engineered Prickly@SpAcDX–PEG–VD1142 for efficient and targeted cancer therapy, which is a very promising and novel nanotherapy that could replace the anticancer drugs. Overall, we envisage that the design of this nanocomposite will open new horizons and bring insights for developing novel and high-efficiency anticancer nanomaterials.

4. Experimental Section

Preparation of the Prickly Zn–CuO nanoparticles: Prickly NPs were prepared through a home-made high intensity ultrasonic device (XH-300UL, Beijing Xianghu Science and Technology development Co., Ltd.) as described previously.[31] Typically, 0.15 g of copper acetate monohydrate and 0.055 g of zinc acetate dehydrate were dissolved in 10 mL of double distilled water by stirring, after which 90 mL of ethanol was added to sustain an ethanol/water solution with a volume ratio of

9:1. After 5 min of sonication, 0.8 mL of ammonium hydroxide (28%–30%) was injected into the reaction cell to adjust the pH to ≈8, and the sonochemical deposition process continued for 1 h (750 W, 100% efficiency). The resultant zinc–copper oxide (Zn–CuO) NPs were then centrifuged and washed twice with double-distilled water and once with ethanol, and then dried under vacuum. The needle Zn–CuO was fabricated according to the above procedure, but using an ethanol/water solution with the volume ratio of 1:9.

Characterization of Prickly NPs: The morphology and dissolution profile of the Prickly NPs at pH 5.0 for 2 h were characterized with HR-TEM (JEM-2100F), operating at 200 kV. The samples were dropped and dried on nickel (Ni) grids to avoid influencing of Cu detection. The element distribution was monitored with EDX mapping. The chemical and crystal components of the Prickly NPs were studied by XPS and XRD. The surface characterization was studied by FTIR at 4000–400 cm^{-1}, using potassium bromide (KBr) tablets. The particle size was determined using DLS with a Zetasizer NanoZS (Malvern Instruments Ltd., UK). The surface zeta (ζ)-potential of the NPs was measured with Zetasizer NanoZS by using disposable folded capillary cells (DTS1070, Malvern, UK). At last, the metal component of Zn–CuO (prickly or rod-like) with the atomic ratio of Cu:Zn was determined by ICP-MS (VISTA-MPX). The NPs (5 mg) were immersed in strong acid (H_2SO_4) (1 M, 5 mL) until completely dissolved; the ion concentrations in the solution were subsequently determined by ICP-MS.

Synthesis of SpAcDX: The SpAcDX was prepared following a previously described protocol.[21,22] Briefly, 1 g of dextran (average molecular weight, MW 9000–11 000; Sigma-Aldrich Co. LLC., USA) was dissolved in 4 mL MilliQ-water and then 0.22 g of sodium periodate (Sigma-Aldrich, USA) was added at room temperature for stirring 5 h to produce partially oxidized dextran. The partially oxidized dextran was further purified by dialysis against distilled water for 5 times through a regenerated cellulose membrane (molecular weight cut-off of 3500 Da). Subsequently, 1.0 g of the lyophilized partially oxidized dextran was modified with 2-methoxypropene (3.4 mL; Sigma-Aldrich, USA), followed by pyridinium *p*-toluenesulfonate (15.6 mg; Sigma-Aldrich, USA) in a dried two-neck round-bottom flask under N_2 protection to yield partially oxidized acetalated dextran. After 1 h, trimethylamine (1 mL; Sigma-Aldrich, USA) was added to terminate the reaction. The reaction mixture was precipitated with 100 mL of MilliQ-water and the sample was collected by centrifugation (16 000 × *g*, 5 min). The pellet was further purified by washing twice with a triethylamine solution (100 mL; 0.01% v/v, pH 8). The sample was dried in vacuum oven at 40 °C for 48 h to remove the residual water and yielding partially oxide AcDX. Subsequently, 1.0 g of partially oxided AcDX was dissolved in 10 mL of anhydrous dimethyl sulfoxide (DMSO, Sigma-Aldrich Co. LLC., USA) and mixed with 4.0 g of spermine at 50 °C for 24 h under stirring. The reduction was performed by adding 2.0 g of $NaBH_4$ to the mixture and incubating at room temperature for another 18 h. The SpAcDX was precipitated in 40 mL of MilliQ water and isolated by centrifugation at 20 000 × *g* for 10 min. The resulting pellet was thoroughly washed with pH 8 MilliQ water for 5 times followed by centrifugation and resuspension cycles. After removal of the residual water through lyophilization, the yield SpAcDX while power was collected and stored at −20 °C.

Synthesis of VD1142: VD1142 was synthesized as described in the previous work.[28] Briefly, 0.2 g of 2,3,5,6-tetrafluoro-4-[(2-hydroxyethyl) sulfonyl] benzenesulfonamide (0.59 mmol) (compound **3d** as described previously)[57] and 0.15 g of cyclooctylamine (1.20 mmol) was dissolved in 1 mL of DMSO and stirred at ambient temperature for 24 h. The mixture was then diluted with 20 mL of ethanol and then extracted with ethyl acetate (3 × 10 mL). The combined organic phase was dried under vacuum and the product was purified through a silica gel column (0.040–0.063 mm) using ethyl acetate:chloroform (1:1) as organic phase.

Fabrication of Prickly@SpAcDX: The 3D microfluidic coflow focusing device was fabricated as described elsewhere.[20] Briefly, borosilicate glass capillaries were assembled on a glass slide. One end of the cylindrical capillary (an inner and outer diameter of around 580 and 1000 µm; World Precision Instruments, Inc., USA) was tapered to a diameter of 20 µm using a micropipette puller (P-97, Sutter Instrument Co., USA); then the orifice diameter was enlarged to 80 µm using sand paper. Subsequently, the tapered capillary was inserted into another cylindrical capillary with an inner and outer diameters of 1100 and 1500 µm (Vitrocom, USA), and coaxially aligned. Two hypodermic needles (Warner Instruments, USA) were situated at the two ends of the outer capillary. A transparent epoxy resin (5 min Epoxi, Devcon) was used to seal the capillaries at the required positions. To encapsulate the Prickly NPs in the SpAcDX polymer, 0.5 mg mL^{-1} of Prickly NPs were mixed with 2.5 mg mL^{-1} of SpAcDX in ethanol as inner phase, and 1% PVA (pH 8) aqueous solution was used as outer phase. The two miscible phases were injected separately into the microfluidic device through polyethylene tubes attached to syringes at flow rates of 2 mL h^{-1} (inner) and 40 mL h^{-1} (outer) controlled by pumps (PHD 2000, Harvard Apparatus, USA). The Prickly@SpAcDX NPs were collected in 0.1% PVA (pH 8) with gentle stirring at 200 rpm. Subsequently, the particles were washed once with MilliQ-water and centrifuged at 10 000 × *g* for 5 min. The Prickly@SpAcDX NPs were stored in pH 8 MilliQ-water at 4 °C.

Construction of Prickly@SpAcDX–PEG–VD1142: To conjugate VD1142 onto Prickly@SpAcDX NPs, the amino group within the NH_2–PEG–COOH first reacted with the hydroxyl group in VD1142 through 1′-carbonyldiimidazole (CDI) mediated amino-coupling reaction. 1 mg of VD1142 (0.002 mmol) was mixed with 0.4 mg of CDI (0.002 mmol) in 5 mL of toluene for 3 h with stirring at 60 °C under argon (Ar) protection. Then, 5 mg of NH_2–PEG–COOH was added to the reaction and kept for another 3 h. The product was dried under vacuum to remove the toluene. Subsequently, the as-prepared VD1142–PEG–COOH was dispersed with 6 mg of NHS and 8 µL of EDC in 2 mL of HEPES acid (pH 5.5) buffer for 2 h. After that, the pH was adjusted to 7.8 and 5 mg of Prickly@SpAcDX NPs were added to the reaction mixture, and kept for another 1 h. The Prickly@SpAcDX–PEG–VD1142 NPs were collected by centrifugation (Sorvall RC 5B plus, Thermo Fisher Scientific, USA) at 10 000 × *g* for 5 min and washed three times with water. The final product was stored in pH 8.0 at 4 °C.

Characterization of Prickly@SpAcDX–PEG–VD1142: The particle morphology and dissolution profile at pH 5.0 were examined by HR-TEM and EDX mapping, as described above. The surface properties of the Prickly NPs, Prickly@SpAcDX, and Prickly@SpAcDX–PEG–VD11, were compared by FTIR. Particle size and surface ζ-potential were measured with Zetasizer NanoZS (Malvern Instruments Ltd., UK). The amount of VD1142 was calculated using fluorescence at Ex/Em of 360/490 nm.

Cell Culture: All the cells in this work were cultured in high glucose (4.5 g L^{-1}) Dulbecco's modified Eagle's medium (DMEM) (EuroClone S.p.A., Italy), supplied with 10% fetal bovine serum (Gibco, Invitrogen, USA), 1% nonessential amino acids, 1% L-glutamine, 100 IU mL^{-1} penicillin, and 100 mg mL^{-1} streptomycin (EuroClone S.p.A., Italy) at 37 °C in an atmosphere of 5% CO_2 and 95% relative humidity.

The hypoxia MCF-7 was induced by incubation with Cobalt(II) chloride ($CoCl_2$; 240 × 10^{-6} M) containing culture medium for 48 h; the medium was changed every 24 h.[44] The expression of CA IX under normoxic and hypoxic condition in MCF-7 cells was monitored with CA IX-specific monoclonal antibody (MAb) M75 (BioScience, Slovakia) and secondary goat antimouse Alexa fluor 488-conjugated IgG antibody (Life Technologies, USA).

The DOX-resistant MCF-7 cells (MCF-7/DOX^R) were selected after sequential exposure of MCF-7 cells to 1–10 µg mL^{-1} of free DOX. The escalating concentration of DOX (1, 2.5, 5, and 10 µg mL^{-1}) was added to culture media containing sensitive MCF-7 cells and kept for 1 d. Then the cells were maintained in medium for 4 d. At each concentration, three cycles were used and then move to next higher concentration cycle.

Expression and Purification of CA IX in Mammalian Cells: The CA IX protein was purified as described elsewhere.[28] Briefly, the DNA fragments, corresponding to the catalytic domain of CA IX (amino acids 38–414) were inserted into a multicloning site of the pCEP4dS vector to construct pCEP4dS-CA IX plasmid. Subsequently, the purified pCEP4dS-CA IX plasmid was transfected to FreeStyle 293-F suspension cells according to the protocol of FreeStyle Max 293 expression system (Invitrogen, Life Technologies). After 5–7 d, the cells were removed by

centrifugation at 6000 × *g* for 20 min, and the secreted recombinant proteins were purified from the supernatant using a CA-affinity column containing *p*-aminomethylbenzenesulfonamide-agarose (Sigma Life Science). The purified CA IX protein was dialyzed into 50×10^{-3} M sodium phosphate buffer (pH 7.0), containing 100×10^{-3} M of NaCl and stored at –80 °C.

Fluorescent Thermal Shift Analysis: FTSA experiments were performed in a Corbett Rotor-Gene 6000 (Qiagen Rotor-Gene Q) instrument. Protein unfolding was monitored by measuring the fluorescence increase of solvatochromic dye 8-anilino-1-naphtalensulfonate (ANS) using blue channel with excitation at 365 ± 20 nm and emission detection at 460 ± 15 nm. Samples contained 4×10^{-6} M of CA IX protein, $0–40 \times 10^{-6}$ M ligand or 0 to 1.5 mg mL^{-1} of NPs, and 50×10^{-6} M of ANS in 50×10^{-3} M of PBS (pH 7.5). Temperature gradient 25–99 °C and the heating rate of 1° min^{-1} was applied. Data analysis was performed as described elsewhere.[58] Briefly, the protein melting temperature (T_m) was determined at each inhibitor concentration and plotted against the total added ligand concentration. K_ds were then determined by the simulation and regression of the ligand dosing T_ms plotted to the equation describing the theoretical function of the melting temperature shift dependence on ligand concentration as previously described.[58,59]

CA IX Inhibition Assay: Applied Photophysics SX.18MV-R stopped-flow spectrometer was used to measure the absorbance change of phenol-red pH indicator at 557 nm.[60] Saturated CO_2 solution was prepared by bubbling the CO_2 gas in MilliQ-water at 25 °C for 1 h. Experiments were performed using 25×10^{-3} M of HEPES buffer containing 50×10^{-3} M of NaCl (pH 7.5), $0–1 \times 10^{-6}$ M inhibitor (or 0–37.5 µg mL^{-1} of NPs) and 30×10^{-6} M phenol-red. CA IX concentration used for inhibition studies was 10×10^{-3} M. Raw curves of absorbance change were analyzed using Origin 8.1 and slope values were used to evaluate the rate of CO_2 hydration. Spontaneous CO_2 hydration rate was used as zero value, and CA IX catalyzed reaction rate was used as maximum value. IC_{50} values were determined using Hill model and inhibition constants were calculated using Cheng–Prusoff equation[61] ($K_i = IC_{50}/(1 + [CO_2]/K_m)$), where $K_m = 7.0 \times 10^{-3}$ M.[62] Experimental values are plotted and the lines corresponding IC_{50} was calculated by Hill equation.

Cell Viability: The cell viability assay was conducted in 3T3 fibroblast cells, hypoxia MCF-7 cells and hypoxia MCF-7/DOX^R cells. 5000 cells were seeded into 96-well plates (PerkinElmer Inc., USA) and allowed to attach overnight. Different particles were added to the cells in DMEM medium at concentrations of 0.1, 0.5, 1, 5, 10, 50, 100, and 500 µg mL^{-1}, and incubated for 24 h. The cells incubated in DMEM and Triton X-100 were used as negative and positive controls, respectively. After particle removal, the wells were washed twice and assayed with CellTiter-Glo Reagent (Promega Corporation, USA). The luminescence was measured by a Varioskan Flash Fluorometer (Thermo Fisher Scientific, USA). All the experiments were performed at least in triplicate.

Confocal and Live Cell Imaging: MCF-7 cells (50 000) were seeded on 35 mm glass-bottomed dishes (MatTek Corporation) and hypoxia condition was created as described above. Then 2 mL of 10 µg mL^{-1} particles were added to the cells for 3 h, and the cells were incubated for another 21 h in medium before imaging. Lysotracker red (DND99, Sigma) was used to stain the lysosomes of the cells according to the manufacture' instructions, and the images were taken with confocal (Leica TCS SP5). In addition, the time-lapse images were acquired with 3I Marianas imaging system (3I intelligent Imaging Innovations), equipped with an inverted spinning disk confocal microscope Zeiss Axio Observer Z1 (Zeiss) and a Yokogawa CSU-X1 M1 confocal scanner. At 2, 12, and 24 h particle treated cell samples were placed in a heated sample chamber (37 °C) and controlled CO_2. A 63 × /1.0 W C-Apochomat Corr WD = 0.28 M27 objective was used and all the images were acquired by a sCMOS (Andor) Neo camera and slideBook 5.0 software (3I intelligent Imaging Innovations). Images were acquired every 2 s. Analyses of the video frames were performed with Fiji Image J.

Flow Cytometry: The targeting ability of VD1142 was also confirmed by flow cytometry experiments. Generally, suspensions of hypoxia MCF-7 cells at the concentration of 2×10^5 cells mL^{-1} were seeded in 6 well plates (2.0 mL per well) and the hypoxia condition was created. Then, different particles at 10 µg mL^{-1} concentration were incubated with the cells for 3 h and the cells were subsequently incubated with medium for another 21 h. After washing with 1× Hank's Balanced Salt Solution (HBSS, pH 7.4), the cells were harvested and fixed with 4% paraformaldehyde (PFA) in $1 \times 6.7 \times 10^{-3}$ M of PBS (pH 7.4) for 20 min at room temperature. Exactly 10 000 events were collected on a LSR II flow cytometer (BD Biosciences, USA) with a laser excitation wavelength of 488 nm using FACS Diva software.

Intracellular Tracking of the NPs by TEM: The cells were incubated with particles under the same condition as flow cytometry. After particle removal, the well was carefully washed with PBS (pH 7.4) and fixed with 4% PFA for 20 min. Subsequently, the wells were washed with PBS, sodium cacodylate buffer (NaCac), and postfixed with 1% osmium tetroxide. The cover glass (placed in the bottom of the 6 well plate) with cells was dehydrated in 30%–100% ethanol for 10 min, embedded in epoxy resin and cut parallel to the cover slide as 60 nm ultrathin sections. The particles in MCF-7 cells were monitored using TEM (Tecnai 12) at 80 kV.

Immunofluorescence Microscopy: Immunofluorescence was done by fixing the hypoxia MCF-7 cells incubated with particles (same protocol as for the TEM samples) with 4% PFA for 20 min, washed three times with Dulbecco, 0.2% of BSA, and permeabilized for 5 min with 0.2% Triton X-100 in PBS. For antibody staining, the permeabilized cells were blocked with Dulbecco plus 0.2% of BSA for 30 min and then incubated with primary antibody for 1 h at 37 °C. The cells were washed with Dulbecco plus 0.2% BSA and incubated with fluorescence-conjugated secondary antibody for another 1 h at room temperature. Cells were mounted in moviol supplemented with DABCO and were imaged using a 63× objective of Leica DM6000B equipped with Hamamatsu Orca-Flash 4.0 V2 sCMOS camera and LAS X software (Leica).

Western Blotting: The hypoxia MCF-7 cells were incubated with particles for 24 h (continuous incubation without particle removal) and then harvested and lysed for 10 min at 4 °C with radioimmunoprecipitation (RIPA) lysis buffer (50×10^{-3} M of Tris, 150×10^{-3} M of, 0.1% of sodium dodecyl sulfate, 0.5% of sodium deoxycholate, 1% of Triton X-100, 1×10^{-3} M of phenylmethylsulfonyl fluoride, 10×10^{-3} M of sodium azide, 10×10^{-3} M of sodium ascorbate, and 5×10^{-3} M of Trolox). The lysates were briefly sonicated prior to centrifugation at 16 000 × *g* for 10 min at 4 °C. Proteins were separated on a 12% of sodium dodecyl sulfate-polyacrylamide gel electrophoresis gel and probed using the indicated antibodies as follow: anti-Calreticulin (Abcam, ab2907) 1:500; anti-Tom 40 (Santa Cruz Biotechnology, #sc-365466) 1:500; anti-*β*-actin (Abcam, #6276) 1:10,000; anti-cleaved caspase 3 (cell signaling technology, #9664) 1:500, and anti-PARP (cell signaling technology, #9542) 1:500. Horseradish peroxidase-linked secondary antibodies (Promega) and enhanced chemiluminescence reagent (Amersham, GE Healthcare) were applied for chemiluminescence detection of the blots.

Copper Release: The copper release experiments were carried out with a Copper Assay Kit (Sigma) according to the manufacture's protocol. The signal was detected by UV-spectrometer at absorbance of 359 nm. The hypoxia MCF-7 cells (1×10^5) incubated with 1 mL of 10 µg mL^{-1} particles were harvested at 3, 6, and 24 h, then the cells were lysed with RIPA buffer and the proteins were pelleted (with Copper Assay Kit supply buffer A) and removed by centrifugation at 16 000 × *g* for 10 min. Subsequently, the Cu^{2+} concentration in cell samples were analyzed with the Copper Assay Kit.

Plasma Stability: The plasma stability of Prickly and Pricly@SpAcDX–PEG–VD1142 particles was evaluated in human serum at 37 °C with continuous magnetic stirring. Triplicate samples were prepared and the particle size, PDI, and *ζ*-potential were measured with Zetasizer NanoZS (Malvern Instruments Ltd., UK).

Supporting Information

Supporting Information is available from the Wiley Online Library or from the author.

Acknowledgements

D.L., L.W., and Z.L. contributed equally to this work. Prof. H. Zhang and Dr. D. Liu acknowledge Jane and Aatos Erkko Foundation (grant nos. 4704010 and 4704482) for financial support. Prof. J. Pan acknowledges the National Natural Science Foundation of China (nos. 21574091 and 21576120). Dr. H. Zhao thanks the financial support from the Academy of Finland (decision no. 266846). A. Janoniene and Dr. V. Petrikaite acknowledge the grant SEN-04/2015 from the Research Council of Lithuania. Prof. H. A. Santos acknowledges financial support from the Academy of Finland (decision nos. 252215 and 281300), the University of Helsinki Research Funds, the Biocentrum Helsinki, and the European Research Council under the European Union's Seventh Framework Programme (FP/2007-2013, grant no. 310892). The authors thank the Electron Microscopy Unit and the Flow Cytometry Unit of the Institute of Biotechnology, University of Helsinki, for providing the necessary laboratory facilities and assistance.

Received: December 9, 2016
Revised: February 4, 2017
Published online:

[1] M. Ferrari, *Nat. Rev. Cancer* **2005**, *5*, 161.
[2] R. A. Burrell, N. McGranahan, J. Bartek, C. Swanton, *Nature* **2013**, *501*, 338.
[3] B. B. Ma, E. P. Hui, T. S. Mok, *Lancet Oncol.* **2010**, *11*, 75.
[4] C. Fedele, R. W. Tothill, G. A. McArthur, *Cancer Discov.* **2014**, *4*, 146.
[5] T. M. Allen, P. R. Cullis, *Science* **2004**, *303*, 1818.
[6] C. de Martel, J. Ferlay, S. Franceschi, J. Vignat, F. Bray, D. Forman, M. Plummer, *Lancet Oncol.* **2012**, *13*, 607.
[7] C. Holohan, S. Van Schaeybroeck, D. B. Longley, P. G. Johnston, *Nat. Rev. Cancer* **2013**, *13*, 714.
[8] N. C. Turner, J. S. Reis-Filho, *Lancet Oncol.* **2012**, *13*, e178.
[9] J. A. Kemp, M. S. Shim, C. Y. Heo, Y. J. Kwon, *Adv. Drug Deliv. Rev.* **2016**, *98*, 3.
[10] C. E. Ashley, E. C. Carnes, G. K. Phillips, D. Padilla, P. N. Durfee, P. A. Brown, T. N. Hanna, J. Liu, B. Phillips, M. B. Carter, N. J. Carroll, X. Jiang, D. R. Dunphy, C. L. Willman, D. N. Petsev, D. G. Evans, A. N. Parikh, B. Chackerian, W. Wharton, D. S. Peabody, C. J. Brinker, *Nat. Mater.* **2011**, *10*, 389.
[11] Y. Guo, D. Wang, Q. Song, T. Wu, X. Zhuang, Y. Bao, M. Kong, Y. Qi, S. Tan, Z. Zhang, *ACS Nano* **2015**, *9*, 6918.
[12] E. Y. Lukianova-Hleb, Y. S. Kim, I. Belatsarkouski, A. M. Gillenwater, B. E. O'Neill, D. O. Lapotko, *Nat. Nanotechnol.* **2016**, *11*, 525.
[13] R. Yuan, H. Xu, X. Liu, Y. Tian, C. Li, X. Chen, S. Su, I. Perelshtein, A. Gedanken, X. Lin, *ACS Appl. Mater. Int.* **2016**, *8*, 31806.
[14] V. T. Pham, V. K. Truong, M. D. Quinn, S. M. Notley, Y. Guo, V. A. Baulin, M. Al Kobaisi, R. J. Crawford, E. P. Ivanova, *ACS Nano* **2015**, *9*, 8458.
[15] H. Song, Y. Ahmad Nor, M. Yu, Y. Yang, J. Zhang, H. Zhang, C. Xu, N. Mitter, C. Yu, *J. Am. Chem. Soc.* **2016**, *138*, 6455.
[16] H. Zhang, D. Liu, M. A. Shahbazi, E. Mäkilä, B. Herranz-Blanco, J. Salonen, J. Hirvonen, H. A. Santos, *Adv. Mater.* **2014**. *26*, 4497.
[17] F. Kong, X. Zhang, H. Zhang, X. Qu, D. Chen, M. Servos, E. Mäkilä, J. Salonen, H. A. Santos, M. Hai, D. A. Weitz, *Adv. Funct. Mater.* **2015**, *25*, 3330.
[18] D. Liu, H. Zhang, B. Herranz-Blanco, E. Mäkilä, V. P. Lehto, J. Salonen, J. Hirvonen, H. A. Santos, *Small* **2014**, *10*, 2029.
[19] D. Liu, S. Cito, Y. Zhang, C.-F. Wang, T. M. Sikanen, H. A. Santos, *Adv. Mater.* **2015**, *27*, 2298.
[20] D. Liu, H. Zhang, E. Mäkilä, J. Fan, B. Herranz-Blanco, C.-F. Wang, R. Rosa, A. J. Ribeiro, J. Salonen, J. Hirvonen, H. A. Santos, *Biomaterials* **2015**, *39*, 249.
[21] E. M. Bachelder, T. T. Beaudette, K. E. Broaders, J. Dashe, J. M. J. Frechet, *J. Am. Chem. Soc.* **2008**, *130*, 10494.
[22] K. E. Broaders, J. A. Cohen, T. T. Beaudette, E. M. Bachelder, J. M. Frechet, *Proc. Natl. Acad. Sci. USA* **2009**, *106*, 5497.
[23] J. L. Cohen, S. Schubert, P. R. Wich, L. Cui, J. A. Cohen, J. L. Mynar, J. M. J. Fréchet, *Bioconjugate Chem.* **2011**, *22*, 1056.
[24] G. De Simone, C. T. Supuran, *Biochim. Biophys. Acta* **2010**, *1804*, 404.
[25] S. Ivanov, S. Y. Liao, A. Ivanova, A. Danilkovitch-Miagkova, N. Tarasova, G. Weirich, M. J. Merrill, M. A. Proescholdt, E. H. Oldfield, J. Lee, J. Zavada, A. Waheed, W. Sly, M. I. Lerman, E. J. Stanbridge, *Am. J. Pathol.* **2001**, *158*, 905.
[26] M. Benej, S. Pastorekova, J. Pastorek, *Subcell. Biochem.* **2014**, *75*, 199.
[27] N. K. Tafreshi, M. C. Lloyd, M. M. Bui, R. J. Gillies, D. L. Morse, *Subcell. Biochem.* **2014**, *75*, 221.
[28] V. Dudutiene, J. Matuliene, A. Smirnov, D. D. Timm, A. Zubriene, L. Baranauskiene, V. Morkunaite, J. Smirnoviene, V. Michailoviene, V. Juozapaitiene, A. Mickeviciute, J. Kazokaite, S. Baksyte, A. Kasiliauskaite, J. Jachno, J. Revuckiene, M. Kisonaite, V. Pilipuityte, E. Ivanauskaite, G. Milinaviciute, V. Smirnovas, V. Petrikaite, V. Kairys, V. Petrauskas, P. Norvaisas, D. Linge, P. Gibieza, E. Capkauskaite, A. Zaksauskas, E. Kazlauskas, E. Manakova, S. Grazulis, J. E. Ladbury, D. Matulis, *J. Med. Chem.* **2014**, *57*, 9435.
[29] V. Dudutiene, A. Zubriene, A. Smirnov, D. D. Timm, J. Smirnoviene, J. Kazokaite, V. Michailoviene, A. Zaksauskas, E. Manakova, S. Grazulis, D. Matulis, *ChemMedChem* **2015**, *10*, 662.
[30] S. Näkki, J. Rytkönen, T. Nissinen, C. Florea, J. Riikonen, P. Ek, H. Zhang, H. A. Santos, A. Närvänen, W. Xu, V.-P. Lehto, *Acta Biomater.* **2015**, *13*, 207.
[31] R. Wu, H. Zhang, J. Pan, H. Zhu, Y. Ma, W. Cui, H. A. Santos, G. Pan, *Adv. Mater. Interfaces* **2016**, *3*, 1600472.
[32] S. Ferdous, F. Liu, D. Wang, T. P. Russell, *Adv. Energy Mater.* **2014**, *4*, 1300834.
[33] W. Chen, H. Zhang, Z. Ma, B. Yang, Z. Li, *J. Mater. Chem. A* **2015**, *3*, 14202.
[34] A. Bera, R. Thapa, K. K. Chattopadhyay, B. Saha, *J. Alloys Compd.* **2015**, *632*, 343.
[35] M. Eshed, J. Lellouche, A. Gedanken, E. Banin, *Adv. Funct. Mater.* **2014**, *24*, 1382.
[36] P. Cronholm, H. L. Karlsson, J. Hedberg, T. A. Lowe, L. Winnberg, K. Elihn, I. O. Wallinder, L. Moller, *Small* **2013**, *9*, 970.
[37] C. A. David, J. Galceran, C. Rey-Castro, J. Puy, E. Companys, J. Salvador, J. Monné, R. Wallace, A. Vakourov, *J. Phys. Chem. C* **2012**, *116*, 11758.
[38] F. H. Niesen, H. Berglund, M. Vedadi, *Nat. Protoc.* **2007**, *2*, 2212.
[39] D. Matulis, J. K. Kranz, F. R. Salemme, M. J. Todd, *Biochemistry* **2005**, *44*, 5258.
[40] M. W. Pantoliano, E. C. Petrella, J. D. Kwasnoski, V. S. Lobanov, J. Myslik, E. Graf, T. Carver, E. Asel, B. A. Springer, P. Lane, F. R. Salemme, *J. Biomol. Screen* **2001**, *6*, 429.
[41] C. T. Supuran, *J. Enzyme Inhib. Med. Chem.* **2012**, *27*, 759.
[42] M. Zat'ovicova, K. Tarabkova, E. Svastova, A. Gibadulinova, V. Mucha, L. Jakubickova, Z. Biesova, M. Rafajova, M. Ortova Gut, S. Parkkila, A. K. Parkkila, A. Waheed, W. S. Sly, I. Horak, J. Pastorek, S. Pastorekova, *J. Immunol. Methods* **2003**, *282*, 117.
[43] S. Jamali, M. Klier, S. Ames, L. F. Barros, R. McKenna, J. W. Deitmer, H. M. Becker, *Sci. Rep.* **2015**, *5*, 13605.
[44] J. Cho, D. Kim, S. Lee, Y. Lee, *Mol. Endocrinol.* **2005**, *19*, 1191.
[45] Z. Chu, K. Miu, P. Lung, S. Zhang, S. Zhao, H.-C. Chang, G. Lin, Q. Li, *Sci. Rep.* **2015**, *5*, 11661.
[46] B. Pelaz, P. del Pino, P. Maffre, R. Hartmann, M. Gallego, S. Rivera-Fernandez, J. M. de la Fuente, G. U. Nienhaus, W. J. Parak, *ACS Nano* **2015**, *9*, 6996.

[47] S. Marrache, S. Dhar, *Proc. Natl. Acad. Sci. USA* **2012**, *109*, 16288.
[48] H. Otera, Y. Taira, C. Horie, Y. Suzuki, H. Suzuki, K. Setoguchi, H. Kato, T. Oka, K. Mihara, *J. Cell Biol.* **2007**, *179*, 1355.
[49] P. Eggleton, E. Bremer, E. Dudek, M. Michalak, *Expert Opin. Ther. Targets* **2016**, *20*, 1137.
[50] D. F. Suen, K. L. Norris, R. J. Youle, *Genes Dev.* **2008**, *22*, 1577.
[51] P. Pinton, C. Giorgi, R. Siviero, E. Zecchini, R. Rizzuto, *Oncogene* **2008**, *27*, 6407.
[52] M. Los, M. Mozoluk, D. Ferrari, A. Stepczynska, C. Stroh, A. Renz, Z. Herceg, Z. Q. Wang, K. Schulze-Osthoff, *Mol. Biol. Cell* **2002**, *13*, 978.
[53] C. Zhang, S. Lee, Y. Peng, E. Bunker, E. Giaime, J. Shen, Z. Zhou, X. Liu, *Curr. Biol.* **2014**, *24*, 1854.
[54] E. S. Alnemri, D. J. Livingston, D. W. Nicholson, G. Salvesen, N. A. Thornberry, W. W. Wong, J. Yuan, *Cell* **1996**, *87*, 171.
[55] S. Ghavami, M. Hashemi, S. R. Ande, B. Yeganeh, W. Xiao, M. Eshraghi, C. J. Bus, K. Kadkhoda, E. Wiechec, A. J. Halayko, M. Los, *J. Med. Genet.* **2009**, *46*, 497.
[56] M. C. Abraham, S. Shaham, *Trends Cell Biol.* **2004**, *14*, 184.
[57] V. Dudutienė, A. Zubrienė, A. Smirnov, J. Gylytė, D. Timm, E. Manakova, S. Gražulis, D. Matulis, *Bioorg. Med. Chem.* **2013**, *21*, 2093.
[58] L. Baranauskiene, M. Hilvo, J. Matuliene, D. Golovenko, E. Manakova, V. Dudutiene, V. Michailoviene, J. Torresan, J. Jachno, S. Parkkila, A. Maresca, C. T. Supuran, S. Grazulis, D. Matulis, *J. Enzyme Inhib. Med. Chem.* **2010**, *25*, 863.
[59] P. Cimmperman, L. Baranauskiene, S. Jachimoviciute, J. Jachno, J. Torresan, V. Michailoviene, J. Matuliene, J. Sereikaite, V. Bumelis, D. Matulis, *Biophys. J.* **2008**, *95*, 3222.
[60] R. G. Khalifah, *J. Biol. Chem.* **1971**, *246*, 2561.
[61] C. Yung-Chi, W. H. Prusoff, *Biochem. Pharmacol.* **1973**, *22*, 3099.
[62] M. Hilvo, L. Baranauskiene, A. M. Salzano, A. Scaloni, D. Matulis, A. Innocenti, A. Scozzafava, S. M. Monti, A. Di Fiore, G. De Simone, M. Lindfors, J. Janis, J. Valjakka, S. Pastorekova, J. Pastorek, M. S. Kulomaa, H. R. Nordlund, C. T. Supuran, S. Parkkila, *J. Biol. Chem.* **2008**, *283*, 27799.